

Fracture Fillings and Intrusive Pyroclasts, Inyo Domes, California

GRANT HEIKEN, KENNETH WOHLETZ, AND JOHN EICHELBERGER¹

Earth and Space Science Division, Los Alamos National Laboratory, Los Alamos, New Mexico

Fractures containing juvenile magmatic pyroclasts were encountered during drilling into a 600-year-old feeder dike beneath the Inyo Domes chain, California. The Inyo Domes consist of a north-south trending, 10-km-long chain of domes, rhyolitic tuff rings, and phreatic craters. Boreholes were cored through the 51-m-diameter conduit of Obsidian Dome, the largest of the Inyo Domes, and through an unvented portion of the intrusion (dike) 1 km to the south. Pyroclast-bearing fractures were intersected in both holes: (1) 7- to 40-cm-thick fractures in welded basaltic scoria and quartz monzonite country rock are adjacent to the conduit at depths of 400-411 m and 492-533 m; they contain gray, clastic deposits, which show truncated cross bedding and convolute bedding; (2) adjacent to the dike, massive fracture fillings occur at depths of 289-302 m (129 m east of the dike) and 366-384 m (95-87 m east of the dike). The fracture fillings consist of mineral clasts derived from the quartz monzonite, quartz monzonitic and basaltic lithic clasts, and juvenile glass pyroclasts. Angular mineral components are present in the same ratio as in the surrounding quartz monzonite country rock. Juvenile glassy and hyalocrystalline pyroclasts make up from less than 1% up to 22% of the deposits. They consist of blocky obsidian clasts, equant, blocky glass pyroclasts with vesicularities of 0-30%, and small pumices with vesicularities of 30-40%. Intrusive pyroclasts differ from erupted pyroclasts in their generally lower vesicularity, higher crystallinity, and the presence of solution pits and clay coatings indicative of prolonged contact with water. The presence, orientation, and texture of fracture fillings strongly resemble those of propped, man-made hydrofractures. We interpret these fractures as naturally occurring hydrofractures. The apparently horizontal fracture orientations may have been controlled by perturbations of maximum principal stress by the dikes or by preexisting sheet fractures in the quartz monzonite country rock. Assumption of elastic moduli and fracturing properties for the Sierran basement rock allows calculation of fluid overpressures 5 to 9 MPa in excess of overburden stress. These overpressures are consistent with either vapor exsolution from decompressed magma or rapid heating of groundwater. However, the textural and chemical similarity of the pyroclasts to phreatomagmatic tephra that appears late in the explosive eruption sequence suggests that heating of groundwater by the dike/conduit caused the fracturing. Such fracturing around volcanic conduits may play an important role in the development of hydrothermal circulation.

INTRODUCTION

The Inyo Domes, California, a chain of rhyolitic tuff rings, phreatic pits, and domes, are among the youngest volcanoes in the conterminous United States, crossing the northwestern edge of Long Valley caldera near the town of Mammoth Lakes (Figure 1). The north-south trending 10-km-long chain has been proposed as the surface expression of a sheetlike rhyolitic dike or dikes [Miller, 1985]. To test the dike hypothesis and investigate processes associated with shallow intrusion, two holes were cored across: (1) the vent of Obsidian Dome and (2) the trend of the chain between Obsidian Dome and the Glass Creek Flow [Eichelberger *et al.*, 1985]. These core holes intersected vented and unvented portions of the underlying dike, respectively.

The conduit hole (RDO-2B) was cored from west to east, the hole sloping toward the east with an initial plunge of 55°, through dome lavas, volcanic ash, moraine deposits, precaldra basalt flows, Sierran plutonic basement, and vent rhyolite (Figure 2). The dike hole (RDO-3A) was cored east to west, plunging initially at 54°, through tephra, moraine deposits, precaldra basalt flows, "basement" quartz monzonite (the nearest exposure is the porphyritic quartz monzonite of Kistler [1966]), and across a rhyolite dike [Eichelberger *et al.*, 1985].

An unexpected discovery during this coring project was

fractures containing juvenile magmatic fragments (pyroclasts) adjacent to the conduit and dike. Such rocks have been reported in only a few localities [Watson, 1968; Andersen and Qvale, 1986], possibly because they are friable and do not survive erosion when exposed.

This study of fracture fillings was made for the purpose of evaluating the eruption phenomena required to form major fracture systems adjacent to the conduit and dike and to determine the genesis and history of the juvenile rhyolitic pyroclasts. Fracturing of country rock during explosive eruptions may be an important process responsible, in part, for fracture permeabilities seen in associated hydrothermal systems. Natural hydraulic fracturing has been addressed and modeled within ancient volcanoes [e.g., Norton, 1984; Nelson and Giles, 1985] and implied as a process leading to hydrothermal eruptions [Nairn and Wiradiviradja, 1980].

We have examined fracture fillings described in unoriented cores from both the conduit and dike holes (RDO-2B and RDO-3A). Selected cores from RDO-3A were mapped by wrapping the core with transparent drafting film to trace lithologic boundaries and fractures. The film was unwrapped and laid flat to produce the cylindrical maps used in this study.

DESCRIPTION OF FRACTURES AND FRACTURE FILLINGS

Table 1 lists samples by core number and a description of their location and relevant characteristics. The fractures and their filling materials are discussed below for the conduit and dike core samples with comparisons to tephra sampled from the tuff ring around Obsidian Dome.

¹Also at Sandia National Laboratories, Albuquerque, New Mexico.

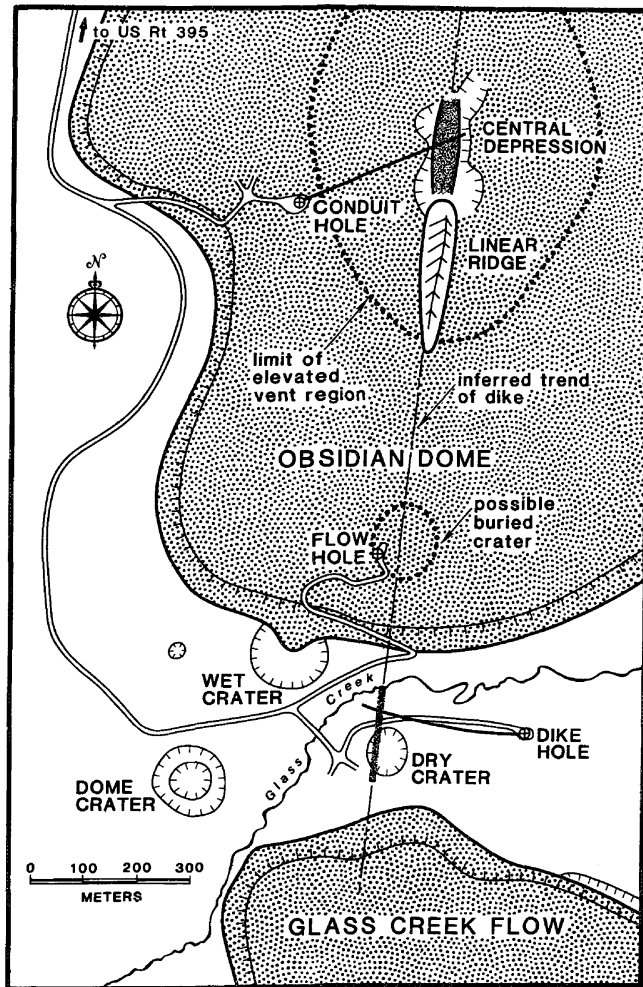


Fig. 1. Obsidian Dome and North and South Glass Creek Domes, Inyo Craters, California, showing location of the core holes RDO-2B (conduit hole) and RDO-3A (dike hole). Rhyolitic domes and phreatic explosion craters are crossed by NNE trending fractures and faults (not shown).

Conduit Hole (RDO-2B)

The 1.4×1.7 km Obsidian Dome and associated tuff ring (mostly buried by the younger dome) are elongate parallel to the chain of Inyo domes and craters and a buried dike [Fink, 1985]. The zone of intrusion beneath Obsidian Dome, filled with rhyolite, is obliquely crossed by the core hole beginning at a depth of 413 m and ending at a depth of 513 m. The zone is 51 m wide and contains a 37-m-wide rhyolite conduit. The other 14 m consists of a fines-depleted breccia containing quartz monzonite, rhyolite, and basalt clasts interpreted as fallback tephra, fractured quartz monzonite screens, and subsidiary rhyolite dikes (Figure 2). West of the conduit the hole traversed basaltic lavas and scoria, and to the east it encountered quartz monzonite. Fractures containing clastic material are intersected by the core hole from about 10 m west to 25 m east of the conduit. These fractures and their clastic fillings were sampled from depths of 396 to 533 m (Table 1). Fractures in welded scoria, located at a depth of 396 to 406 m and from the conduit boundary to 9.4 m west of the conduit, contain gray, bedded fill, ranging in thickness from 7 to 40 cm. Bedding in the fracture fills is varied, from truncated cross bedding to convolute bedding (Figure 3). Rotation of the core

about its axis until foreset beds are properly oriented shows that the fractures are nearly horizontal (Figure 3).

Fractures radiating outward from the eastern side of the conduit are irregular and not well defined (recovery was incomplete because the host rock is laced with fractures and much of the fracture filling was carried away during coring). Fracture fillings were sampled from depths of 491 m to 533 m, as far as 24 m to the east of the conduit.

Dike Hole (RDO-3A)

This core hole crossed the Inyo dike at a depth of 626 m and went back into quartz monzonite country rock at 650 m; at this depth, the dike is 8 m wide. Coring was stopped 30 m west of the dike at a depth of 759 m. Fracture fills were first encountered at a depth of 289 m, 129 m east of the dike. The deepest fracture fillings were observed at a depth of 384 m; all of these fractures are within quartz monzonite (Table 1).

Unlike the bedded fracture fillings adjacent to the conduit, those from the dike core hole are massive. Shallower fracture fillings (depth ≈ 290 m; distance from dike ≈ 128 m) are present in fracture networks composed of subhorizontal to near-vertical fractures (Figure 3). Fracture surfaces are rough and irregular, with rare slickensides. Larger clasts are concentrated near the centers of the fillings and define a crude graded bedding, not at all like the well-bedded deposits in fractures adjacent to the conduit. Fracture networks consist of both unfilled and filled fractures with fracture fillings 0.4 to 8 cm thick. There were no sedimentary structures that could be used to orient the cores.

Composition of Fracture Fillings

The fracture fillings are composed of three sets of particle types (Figures 4–7): (1) mineral clasts derived from comminuted quartz monzonite, (2) juvenile glass pyroclasts, and (3) lithic clasts consisting of quartz monzonite and basalt. Mineral clasts make up most of these deposits (Table 2).

Mineral clasts. Mineral clasts consist of the following:

1. Unzoned, perthitic potassium feldspars make up some mineral clasts; most are subangular to subrounded grains and range in size from 20 μm to 2 mm.
2. Plagioclase clasts are mostly $<300 \mu\text{m}$ but are as long as 2 mm. Cores of some grains have been replaced by calcite.
3. Subrounded quartz clasts are equant to slightly elongate, in the size range of 20 μm to 2 mm. Many are fractured and/or chipped and exhibit undulate extinction under polarized light.
4. Ragged "shredded," elongate, 40-to 400- μm -long biotite grains are distributed throughout the fracture fillings and are an important part of the finer-grained matrix (Figure 5).
5. Minor components include Fe-Ti oxides (equant, subhedral grains in the size range of 40–400 μm) and traces of hornblende, zircon, and aegerine-augite.

Mineral components of the fracture fills are present in approximately the same ratio as in the surrounding quartz monzonite (Table 3). Exceptions exist within the conduit hole, where mineral components are derived from quartz monzonite but the fractures are located in welded basaltic scoria.

All of the coarser particles are enclosed, at least in part, by a fine-grained matrix ($<40 \mu\text{m}$). This "rock flour" is composed of the same mineral and glass clasts and in approximately the same ratio as the coarser components described in the mode of Table 3. The smallest clasts are in the size range of 4–6 μm (Figure 5).

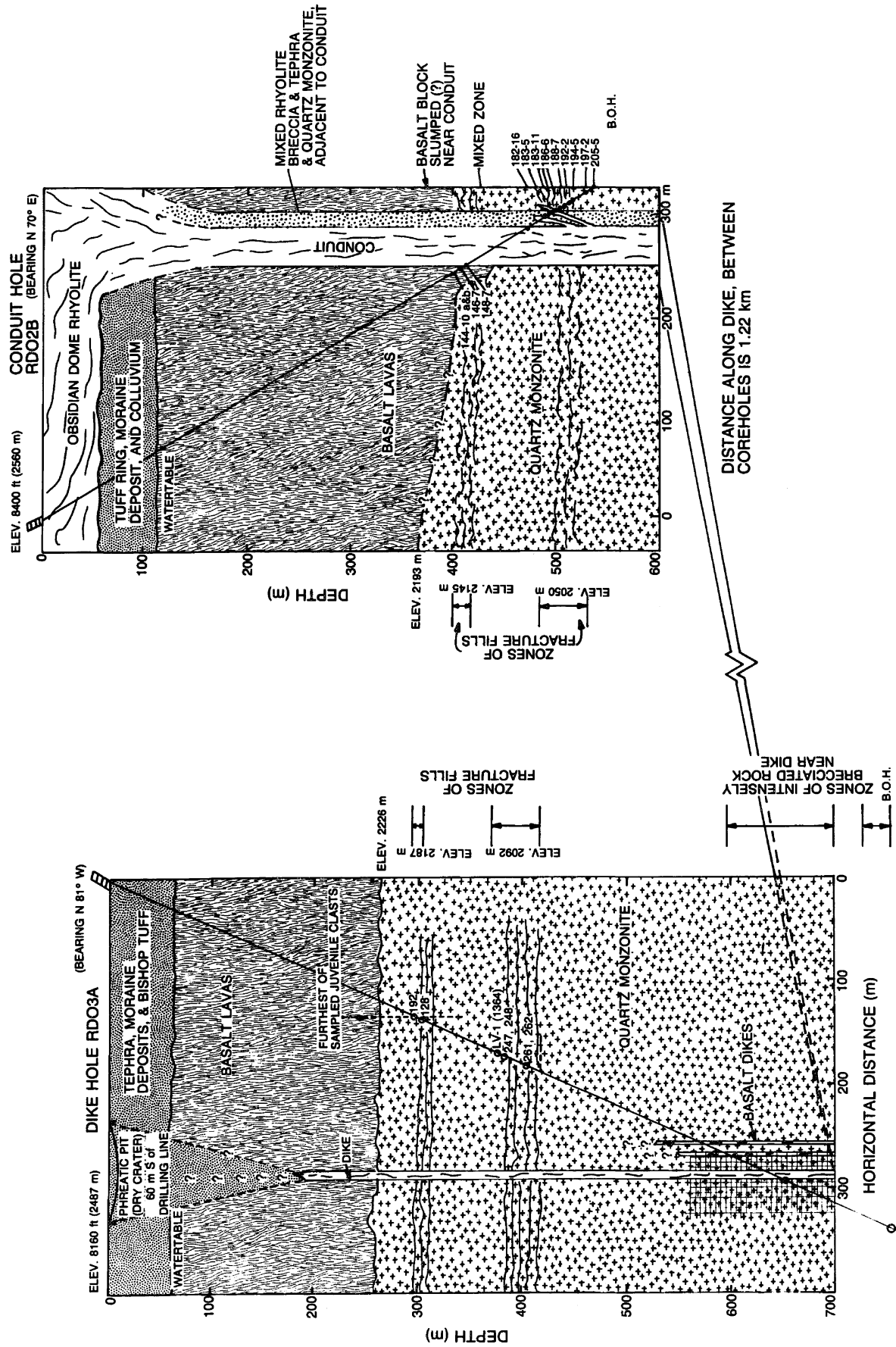


Fig. 2. Cross sections through the Obsidian Dome conduit and the rhyolite dike between Obsidian Dome and South Glass Creek Dome. Cross sections are drawn along the surface of the core holes RDO-2B and RDO-3A. Zones of fractures and fracture fillings are located in quartz monzonitic country rock and basaltic lavas.

TABLE 1. Description of Pyroclast-Bearing Fragmental Samples From Dike Core (RDO-3A) and Conduit Core (RDO-2B)

Core	Depth,* m	Distance,* m	Comments	Glass Clasts
<i>RDO-2B (Conduit)</i>				
144-10A	396	9.4 W	in welded, basaltic scoria	yes
144-10B	396	9.4 W	well bedded	yes
146-7A	400	6.7 W	4–40 cm thick, well bedded, coarse	no
146-7B	400	6.7 W	in welded scoria, 4–40 cm thick, at granite/basalt contact	yes
148-7A	406	4.0 W	in basalt, 7 cm thick, bedded	trace
182-16	491	3.7 E (1.1 W)	authigenic minerals, especially clays	no
183-5	492	4.4 E (0.5 W)	authigenic minerals, especially clays	no
183-11	493	4.5 E (0.3 W)	authigenic minerals, especially clays	no
186-6	500	7.8 E (0.2 E)	authigenic minerals, especially clays	no
188-7	504	10 E (2.4 E)	authigenic minerals, especially clays	no
192-2	512	13.8 E	clast-bearing margin of rhyolite finger	no
194-5	514	14.8 E (0.3 E)	in quartz monzonite	no
197-2	520	17.6 E (3.1 E)	in quartz monzonite	no
205-5	533	24.2 E (9.7 E)	in quartz monzonite	no
<i>RDO-3A (Dike)</i>				
128-4A	290	128 E	0.4–0.8 cm thick	yes
128-5A	290	128 E	up to 8 cm thick	yes
128-6A	290	128 E	2.5 cm thick	yes
192-7A	289	129 E	up to 6 cm thick	yes
247-7A	366	95 E	7 cm thick	yes
247-7B	366	95 E	up to 4 cm thick	yes
248-2A-1	366	95 E	up to 8 cm thick, fracture side	yes
248-2A-2	366	95 E	up to 8 cm thick, fracture center	yes
261-1A	384	87 E	up to 8 cm thick	yes
261-7A	384	87 E	up to 4 cm thick	no

*Vertical depth from surface and horizontal distance west (W) and east (E) from conduit or dike. For conduit samples, the shortest horizontal distance to an intact (nonfragmental) intrusive rock is indicated in parentheses.

Glass pyroclasts. Of 25 samples from fracture fills (both core holes), 15 contained blocky glass clasts. Most are less than 1 mm in diameter but range in size from $<10\ \mu\text{m}$ to 1.6 mm; coarser clasts are rare. Most have $<30\%$ vesicles by volume.

Quench textures exhibited by juvenile pyroclasts are composed mostly of 5- to $10\text{-}\mu\text{m}$ -long feldspars surrounded by rhyolitic glass. The tabular crystals rise about $1\ \mu\text{m}$ above the glassy clast surfaces (Figure 7). Most crystals are subparallel and appear to follow flow banding developed within the magma before fragmentation. Most of the quench crystals at grain surfaces appear to have grown after fragmentation; none are cut by those surfaces but appear to have been forced through those surfaces by continued crystal growth. In this section these quench crystals are optically continuous from the interior to above the glass surface. Quench crystals are common in pyroclasts from the dike fracture fillings and range in composition from An_{16} to An_{28} (Table 4). However, quench crystals are rare in pyroclasts from fillings adjacent to the conduit and have sanidine compositions.

Major element chemical compositions of glass separates listed in Table 5 show two families of glass compositions: rhyolite ($\text{SiO}_2 \approx 73$ to 74 wt %) and rhyodacite ($\text{SiO}_2 \approx 69$ to 72 wt %). As mentioned below, these two families are associ-

ated with elongate and spherical vesicle shapes, respectively, especially evident in Obsidian Dome tephra.

Conduit hole (RDO-2B): Fracture fillings sampled close to the western side of the conduit, at depths of 396–406 m and from the conduit edge to 9.4 m west of the conduit, all contain glass pyroclasts (trace to 22%). Pyroclasts are mostly equant, blocky and contain 0 to 30% small spherical to ovoid vesicles. Rare micropumices are characterized by parallel, tubular vesicles (Figure 5). Most of the micropumices described are all glass, but some contain small K-feldspar and Fe-Ti oxide phenocrysts. Pyroclast surfaces are covered with concave solution pits, 3– $10\ \mu\text{m}$ in diameter and $\sim 1\ \mu\text{m}$ deep.

Average analyses for core, surface, and bulk pyroclast samples are presented in Table 5. It was difficult to obtain reliable analyses of fracture-filling pyroclasts because of small size and extensive hydration. Therefore detailed chemical comparisons are not possible. However, data from the pyroclasts generally resemble the rhyolite compositions of the dike, conduit, and tuff ring, but they do not resemble the silica-poor, titanium-rich rhyodacite component that is present in the conduit and tuff ring.

Dike hole (RDO-3A): Whereas all pyroclasts from fractures intersected near the dike hole are hyalocrystalline, with the volume of glass ranging from $\sim 30\%$ to $\sim 70\%$ for any

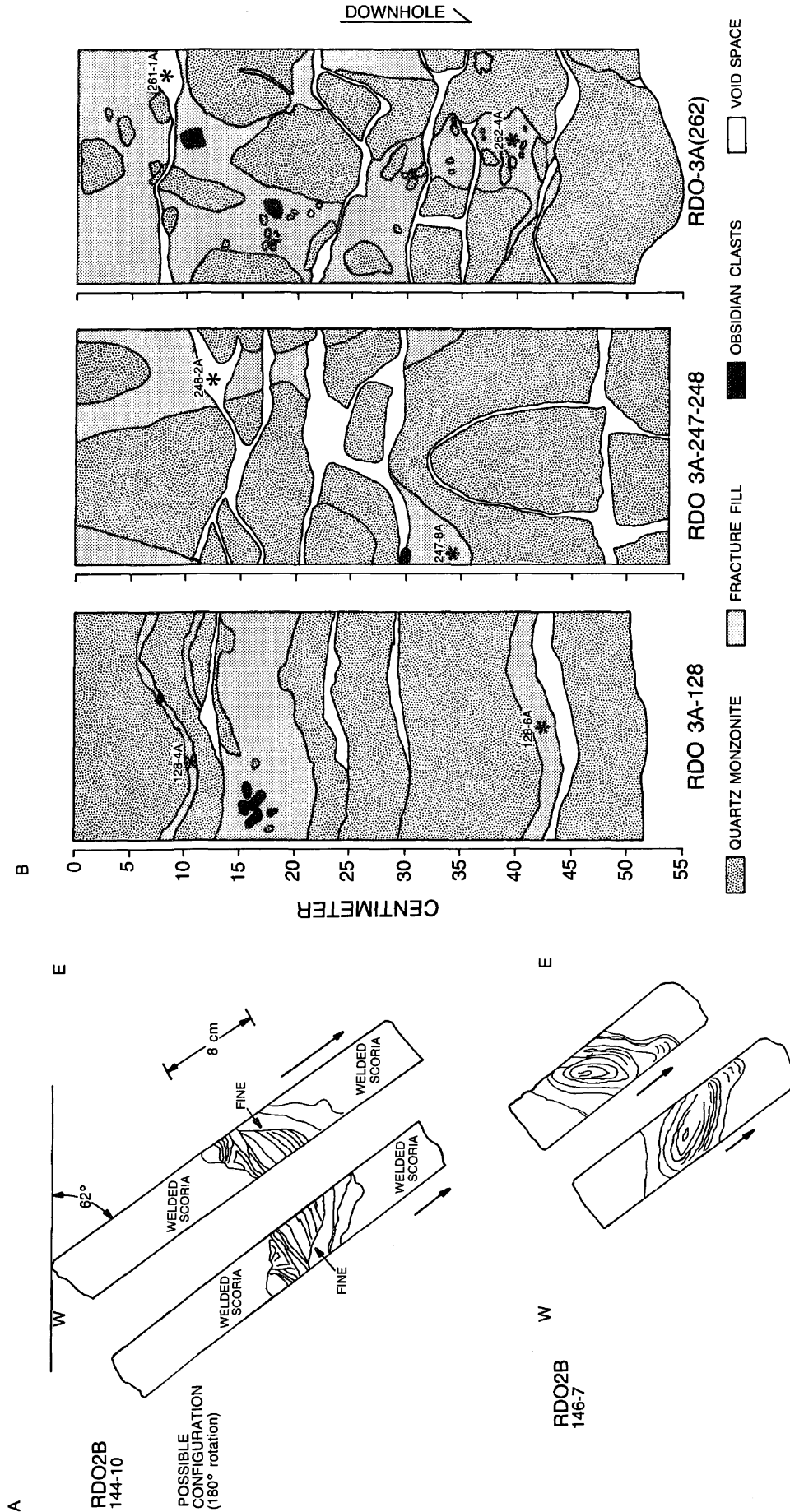


Fig. 3. Sketches of cores containing clastic fracture fillings. (a) RDO-2B. Sketches of core segments located 5 m and 1 m west of the conduit. The gray, bedded deposits range in thickness from 7 to 40 cm. The bedding includes cross beds, convolute bedding, and truncated bedding parallel to fracture surfaces. Two possible orientations of the core are shown; the lower orientations best fit the models for emplacement of the cross-bedded fracture fillings. (b) RDO-3A. Core maps (drawn on mylar sheets wrapped around the core, then lain flat as the "map") of cores from the dike hole. See Figure 2 for locations of these cores. These deposits are massive, with coarser obsidian clasts present in the center of each fracture. Asterisks represent sample locations.

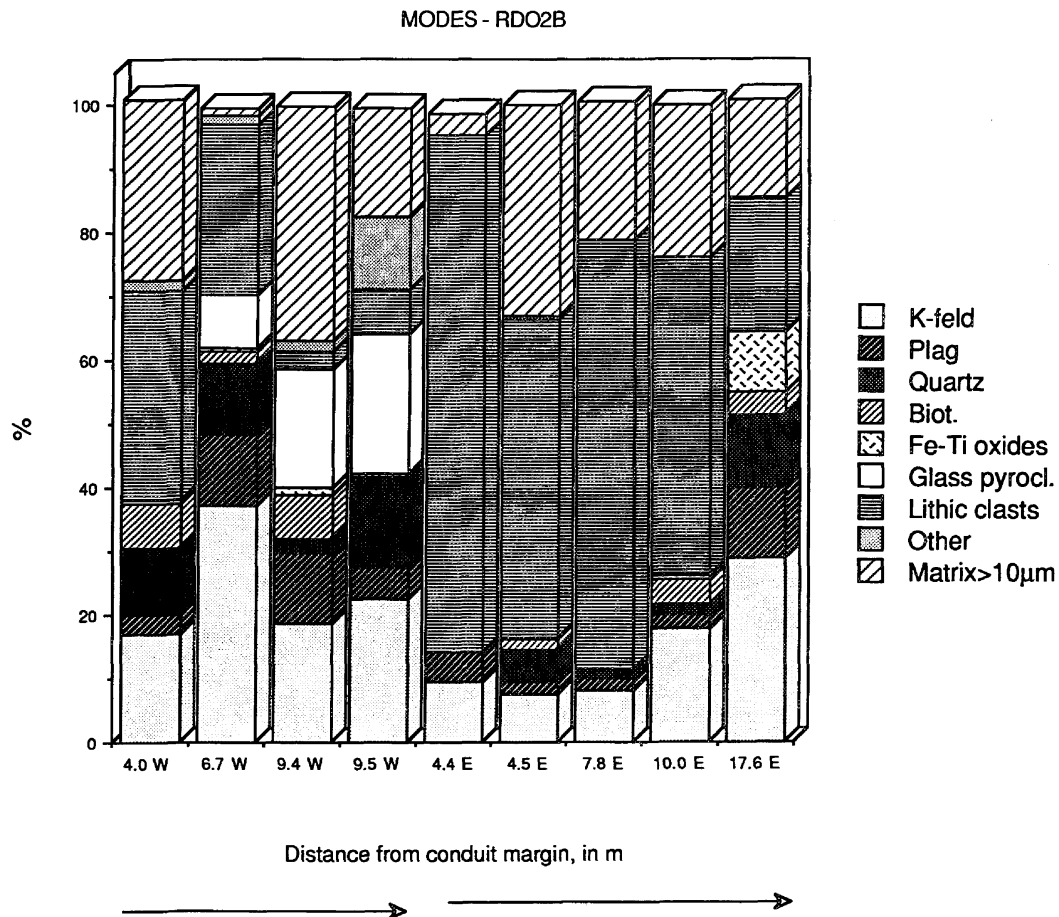


Fig. 4. Bar graph showing variation in modes of fracture-filling deposits with distance from the vent (RDO-2B).

individual pyroclast, most pyroclasts adjacent to the conduit are glass. The X ray fluorescence analyses of bulk glass separates indicate that the composition of glass pyroclasts in fracture fills over 120 m from the dike are nearly identical to rhyolite compositions in the dike.

Pyroclast shapes range from cubic to tabular, and clast surfaces from planar to irregular. Vesicle shapes range from smooth, flattened ovoids to ragged voids that are made up of coalesced vesicles. Vesicle sizes range from 1 μm to 60 μm long. Some clasts have a diktytaxitic texture, with irregular voids and patches of glass between crystals.

Obsidian Dome Tephra

Samples of Obsidian Dome tephra were included in the study for comparison with those found in cores. These samples, which came from the inner edge of the tephra ring just west of the dome (Figure 4) and from a section located 1.5 km to the northeast, represent tephra believed to have been explosively erupted from the conduit prior to emplacement of dome lavas. Miller [1985] estimates that the tephra represents about 0.02 km³ of magma, which is about one-eighth the dome volume.

Figure 8 shows the stratigraphic column for the tephra ring section mentioned above. Sample 1 was taken from a pumiceous subplinian fallout layer, while samples 2 and 3 were taken from planar-bedded and massive-bedded surge layers, respectively. The subplinian layer is believed to represent a magmatic stage of the eruption, while the planar- and massive-bedded deposits show textures that indicate they are

products of phreatomagmatic origin [Wohletz, 1987; Heiken and Wohletz, 1985]. A similar sequence is visible in the section northeast of the vent.

Results of grain size analysis are shown in Figure 8 as size frequency histograms. The size data are represented in these histograms as a cubic spline curve, which passes through points corresponding to weight fraction measured in sieves nested at half-phi intervals ($\phi = -\log_2 \text{mm}$). An important feature of these data is that the distributions are polymodal, especially those of samples 2 and 3. The polymodality of tephra size distributions is analyzed and discussed by Sheridan *et al.* [1986], and we use that method to interpret subpopulations in our data. Sample 1 shows one significant mode (subpopulation 1), which we feel is characteristic of fallout materials close to the vent. In contrast, samples 2 and 3 have significant modes of subpopulations 2, 3, and 4, which show the relative contributions of particles carried in grain flow, saltation, and suspension. Because of the complexities of tephra transport during explosive eruptions and the strong effect of transport mechanism on size distribution, the size data are difficult to correlate to pyroclast sizes observed in fracture fills; subpopulation 4, however, is most similar in apparent size distribution and may best correlate with fracture fill materials (Tables 3 and 4).

The juvenile glassy pyroclasts are illustrated by scanning electron micrographs showing dominant textural features: vesicles, surface alteration, and grain angularity. Figure 9 shows a sequence of photos of the subplinian ash (1, bottom photographs), planar surge (2, middle), and massive surge (3, top). A

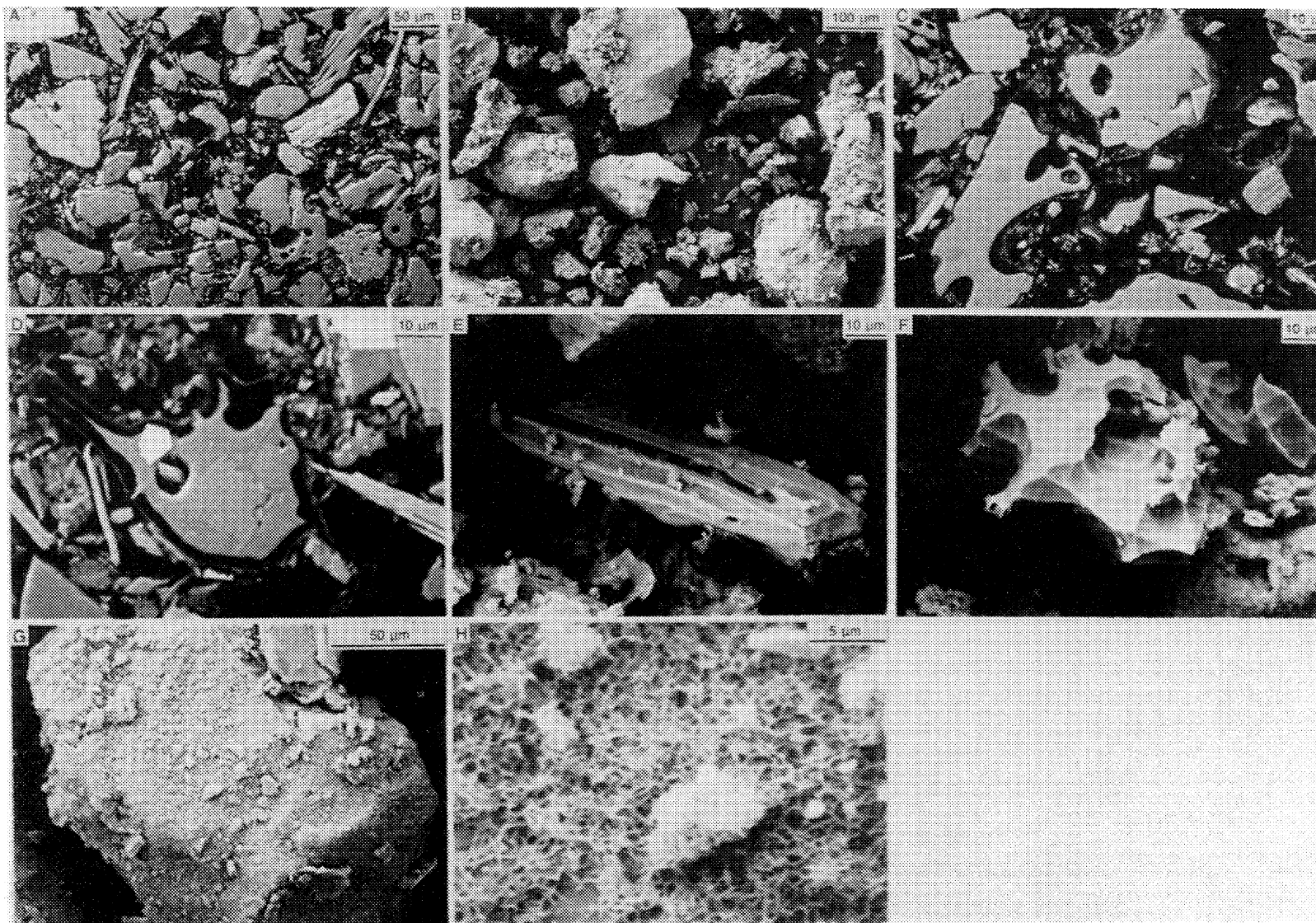


Fig. 5. Scanning electron micrographs of clasts from RDO-2B. (a) Thin section. Particles consist mostly of comminuted quartz monzonite (81%, including K-feldspar, plagioclase, quartz, biotite, Fe-Ti oxides, and quartz monzonite fragments); 19% of the fill consists of blocky, vesicular glass clasts. (b) Comminuted quartz monzonite and glass clasts. The fine-grained matrix coating the larger clasts is "rock flour" with the same ratio of mineral clasts as the coarser fraction. (c) Thin section. Mostly blocky, vesicular rhyolitic glass clasts, surrounded by fine-grained mineral grains. (d) Partly vesicular, porphyritic glass clast. Flat light-colored clasts are biotite grains. (e) Pumice pyroclast with elongated parallel vesicles. (f) Vesicular glass pyroclasts. Surfaces of these pyroclasts are covered with solution pits. Most of the glass clasts in deposits located near the conduit appear to have been pitted during interaction with water. (g) Mineral clast coated with smectite clays. (h) Closeup of the grain surface in Figure 5g.

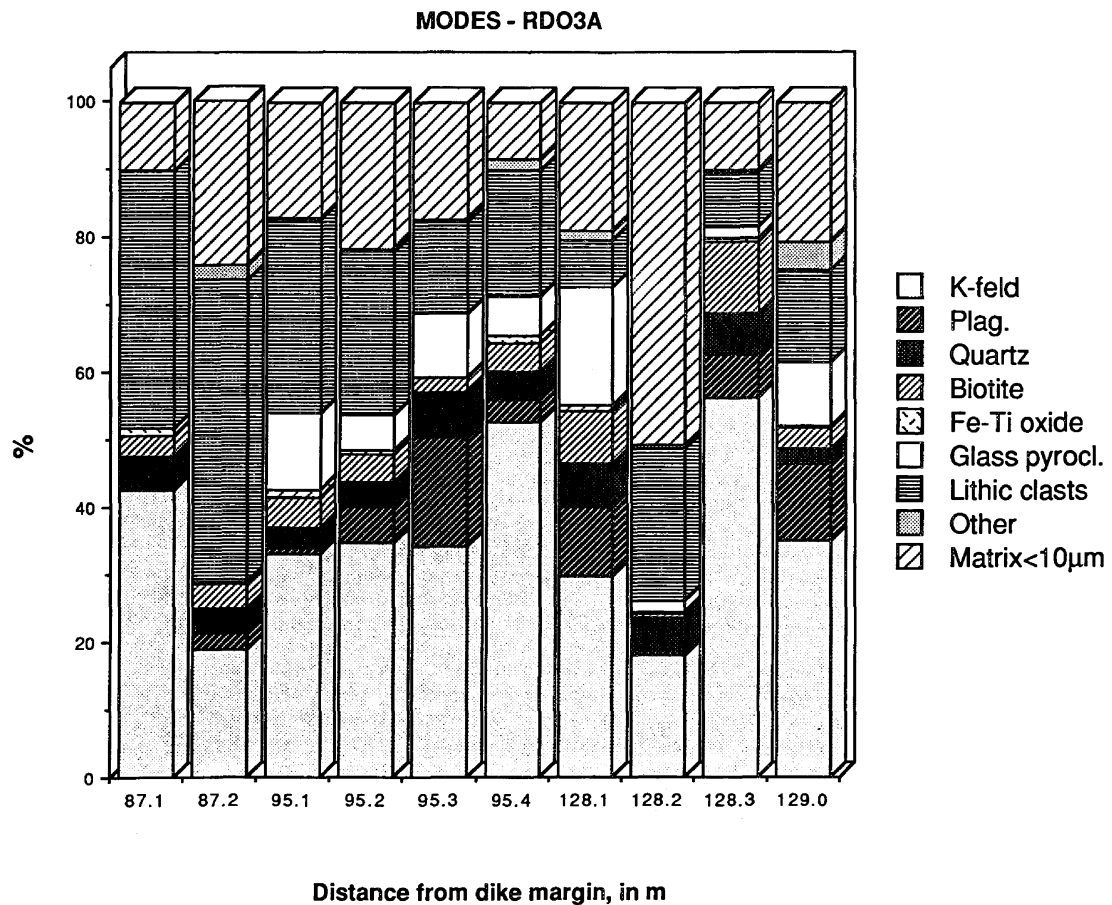


Fig. 6. Bar graph of modes of fracture fillings with increasing distance from the dike, RDO-3A.

rhyolitic and rhyodacitic example are shown for each sample on the left and right, respectively. Compositions, determined by energy dispersive spectral analysis of grain surfaces, are listed in Table 5 for Obsidian Dome tephra. Vesicle shapes vary from stretched and elongated for rhyolitic pyroclasts to nearly spherical for those with rhyodacitic compositions. Grain rounding, blockiness, and surface alteration (and surface aggregation of smaller particles), greater for sample 2 and greatest for sample 3, are caused by the interaction with meteoric water during magma fragmentation. Lithic fragments found in tephra are mostly quartz monzonite and decrease upward in the sampled section from 7 vol. % to about 2 vol. %; crystal abundances likewise decrease upward in the section. Overall, Obsidian Dome tephra are very similar in texture and composition to fracture-filling juvenile pyroclasts except that rhyodacite pyroclasts have not been confidently identified in the latter.

NATURAL HYDRAULIC FRACTURING

Hydraulic fracturing (hydrofracturing) has been suggested by Julian [1983] and Julian and Simpkin [1985] to occur naturally during some magma intrusions in the earth's crust. Furthermore, tensile crack formation has been observed in the natural geothermal environment in Iceland by Foulger and Long [1984]. Many workers have attributed long-period seismic events and harmonic tremor to fluid-driven fracturing [e.g., Fehler, 1983; Chouet, 1986]. Ground surface deformation (tilt) is commonly observed during man-made hydrofracturing

[Sun, 1969] and has been attributed to hydrofracturing in volcanoes by pressurized phreatic fluids [West *et al.*, 1978]. The observations we have described here can also be interpreted in light of the hydrofracturing process. The many descriptions of hydrofracturing mechanics [e.g., Hubbert and Willis, 1957; Howard and Fast, 1970; Chouet and Julian, 1985], together with observations of man-made hydrofractures, enable certain inferences to be made about the Inyo fracture fillings.

Granular materials are commonly added to fluids during well stimulation by hydraulic fracturing in oilfields so that these materials may prop open fractures. Sand is a common proppant material because it keeps newly formed fractures open after borehole depressurization and maintains a sufficient permeability for fracture extension during reinjections [Warpinski *et al.*, 1981]. Because material from the Inyo dike is observed in fractures and shows bedding similar to experimental hydrofracture proppants, fluid evidently flowed from the dike through the fracture. The origin of the observed bedding is discussed later in this report.

The explosive products of Obsidian Dome indicate that early extruded magma contained volatile overpressures. Eichelberger *et al.* [1986] discuss magma water saturation and degassing during both explosive and effusive stages of dome growth. They maintain that magmatic vapor overpressures (pressures greater than lithostatic) up to ~50 MPa initially existed in the conduit. For hydrofracturing to have occurred, these overpressures must have been sufficient to overcome the tensile strength of the quartz monzonite (maximum) or opening of preexisting fractures (minimum).

TABLE 2. Modes of Fracture Fill Constituents

Sample	K-Feldspar	Plagio-clase	Quartz	Biotite	Fe-Ti Oxides	Lithic Glass	Matrix Clasts < 10 μm	Comments	
<i>RDO-2B</i>									
144-10A	18.6	11.0	2.3	6.9	1.1	18.6	2.9	36.6	matrix in coarser material and as beds is mostly rock < 10 μm ; small blocky pyrite
144-10B	22.6	4.9	14.1	0.7	0.0	21.9	7.0	17.0	quartz monzonite and basalt lithics
146-7B	37.2	11.1	11.1	1.9	0.6	8.4	26.7	1.3	quartz monzonite and basalt lithics
148-7A 182-16*	17.0	2.9	10.6	7.0	0.0	0.6	32.7	28.1	quartz monzonite lithics no mode count; basaltic clasts are altered; no glass
183-5	9.4	4.7	83.3	3.1	mostly basalt and some quartz monzonite lithics
183-11	7.5	2.0	5.0	1.5	0.5	...	50.0	33.0	altered basalt clasts
186-6	8.0	2.0	1.5	67.5	21.6	mostly quartz monzonite and some basalt lithics
188-7	17.8	2.2	1.7	3.9	0.6	...	50.0	23.9	mostly basalt lithics and some calcite cement
192-2	28.5	10.5	11.5	3.5	9.5	0.0	21.0	15.5	equal amounts of basalt and quartz monzonite clasts
<i>RDO-3A</i>									
128-4A	29.6	10.3	6.6	7.6	1.0	17.3	7.0	19.0	quench crystals throughout glass (hyalocrystalline)
128-5A	18.0	0.6	5.0	0.6	0.3	1.6	22.6	50.3	finely fragmented (more than other samples)
128-6A	56.0	6.6	6.0	10.6	0.6	1.6	8.0	10.0	
192-7A	35.0	11.3	2.3	3.0	0.3	9.6	13.6	20.3	blocky hyalocrystalline clasts, some with brown 5- μm -diameter spheres on surfaces
247-7A	33.0	1.0	3.0	4.3	1.3	11.3	28.6	17.0	
247-8A	34.6	5.3	3.6	4.3	0.6	5.3	24.0	21.6	
248-2A	34.3	16.0	6.6	2.3	...	9.3	13.6	17.3	
261-1A	52.6	3.3	4.0	4.3	1.0	6.0	18.6	8.3	matrix has abundant brown < 5- μm -diameter spheres (clays?)
261-7A	42.6	0.3	4.6	3.0	1.3	0.0	38.8	10.0	spheres, < 5- μm -diameter, in matrix and complete alteration of some Fe-Ti oxides
262-4A	19.0	2.3	3.6	...	0.3	...	44.6	24.3	

*Plagioclase > K-feldspar > biotite/hornblende.

Fracture Orientations

Two lines of evidence suggest that at least some of the observed fractures are horizontal:

1. Orientation of the fracture-filling cross bedding with respect to the core axis is consistent with horizontal fracture planes.

2. Most fractures were encountered in the horizontally bedded basalt section and the uppermost quartz monzonite where preexisting horizontally oriented sheet fractures (exfoliation fractures) should be most abundant [Johnson, 1970].

For the dike hole the postulated horizontal fractures minimize the distance for transport of pyroclasts, which were found as far as 128 m from the single intrusion encountered in the core hole. Pollard *et al.* [1983] find that dike emplacement may locally perturb the regional stress field in a way that near the dike, maximum principal stress is oriented horizontally (Figure 10). This perturbation would be evidenced by a set of horizontally oriented fractures, caused by intrusion-related

TABLE 3. Comparison of Modes From Clastic Fracture Fill (RDO-3A, Sample 1364b, Depth of 363 m, 94 m East of the Dike) and Adjacent Quartz Monzonite Country Rock (500 Points Each)

	Mode Fracture Fill, %	Mode Recalculated Without Matrix, Lithics, and Glass	Mode Quartz Monzonite
K-feldspar	20.8	50.7	39.3
Plagioclase	5.2	12.7	27.1
Quartz	9.6	23.4	27.6
Biotite	3.6	8.8	4.8
Fe-Ti oxides	1.0	2.4	0.3
Hornblende	0.2	0.5	trace
Lithic clasts	5.2
Matrix*	45.4
Allanite	0.2	0.5	0.3
Glass pyroclasts	8.4
Sphene	0.4	1.0	trace

*Particles < 40 μm .

TABLE 4. Major Element Compositions of Feldspar Quench Crystals in Glassy Pyroclasts From Fracture Fillings

	RDO-2B 144-10A	RDO-3A 128-6A	RDO-3A 192-7A	RDO-3A 261-1A
SiO ₂	66.33	64.37	64.59	61.33
TiO ₂	0.02	0.01	...	0.03
ZrO ₂	0.04	0.01	...	0.09
Al ₂ O ₃	19.36	22.40	22.64	24.67
FeO	1.14	0.17	0.13	0.26
MnO	...	0.01
MgO	0.01	...
CaO	0.51	3.43	3.81	6.10
NiO	0.09	0.12
BaO	0.26	0.07
Na ₂ O	4.93	9.55	9.33	8.02
K ₂ O	8.65	0.12	0.21	0.25
Total	100.24	100.07	101.07	100.94
Analyses	2	4	4	4
An	2.31	16.08	17.71	28.51
Ab	43.15	81.65	79.82	68.43
Or	49.95	0.71	1.17	1.42

fracturing, cutting an earlier set of vertically oriented fractures along which the dike intruded.

The Fracturing Process

Conditions of fracture propagation are readily calculated for horizontal fractures. We have found good agreement among the hydrofracture models presented by Sun [1969],

Geertsma and Haafkens [1979], and Spence and Turcotte [1985]. Sun [1969] solves the problem of calculating uplift from hydraulically induced fractures by considering the equilibrium distribution of stresses and displacements in a semi-infinite medium. By assuming a thin disk-shaped fracture and building upon Green's [1949] analysis of fracturing in an infinite medium, Sun finds the displacements from general equations of equilibrium for an isotropic elastic body [Love, 1939] using an image method for boundary conditions at a free surface. His relationships among fracture dimensions, fluid overpressure, and host rock elastic properties are

$$\frac{X}{l} = \left[1 - \left(\frac{p - \rho gh}{p} \right)^2 \right]^{1/2}$$

$$p = \rho gh + \frac{w\pi E}{8(1 - \nu^2)(X^2/l)}$$

$$q = \frac{16l^3(1 - \nu^2)(X/l)^5(p - \rho gh)}{3E}$$

These expressions were numerically solved for four unknowns using an additional expression from Geertsma and Haafkens [1979] for an approximately elliptical fracture:

$$p = \rho gh + \frac{w\mu}{2(1 - \nu)X[1 - (X/l)^2]^{1/2}}$$

In the above expressions, p is total fluid pressure, ρ is the host rock density, h is the fracture depth, g is gravitational accel-

TABLE 5. Major Element Compositions of Obsidian and Glassy Pyroclasts

Sample Type*	SiO ₂	TiO ₂	Al ₂ O ₃	FeO _x †	MnO	MgO	CaO	Na ₂ O	K ₂ O	Total	Number	Type of Analysis
<i>RDO-2B Conduit and "Fingers" (Crystalline)</i>												
RhD	69.96	0.36	15.47	2.66	0.05	0.47	1.53	4.58	4.83	99.91	7	XRF
Rhy	73.17	0.14	14.35	1.82	0.05	0.11	0.76	4.35	5.25	100.00	4	XRF
F-1	71.22	0.22	14.65	2.25	0.06	0.19	1.15	4.45	5.09	99.82	9	XRF
F-2	72.48	0.15	14.21	1.87	0.05	0.13	0.85	4.35	5.30	99.39	6	XRF
F-3	72.62	0.15	14.18	1.87	0.05	0.08	0.85	4.32	5.28	99.40	5	XRF
<i>RDO-2B Fracture Filling Glass Pyroclasts</i>												
144-10A	73.19	0.06	12.75	1.14	0.00	0.04	0.60	2.38	2.82	93.05	6	EPM
144-10B	72.20	0.11	13.30	1.43	0.04	0.09	0.74	2.30	2.49	92.74	7	EPM
146-7B	72.65	0.03	13.18	1.14	0.04	0.03	0.68	3.06	2.80	93.91	6	EPM
<i>RDO-3A Dike Vitrophyre</i>												
Dike	73.61	0.14	13.98	1.80	0.05	0.05	0.73	4.32	5.29	99.97	25	XRF
<i>RDO-3A Fracture Filling Glass Pyroclasts</i>												
128-4A	73.93	0.17	12.84	0.81	0.03	0.01	0.53	3.04	1.94	93.32	5	EPM
192-7A	73.35	0.14	14.31	1.80	0.06	0.07	0.74	4.28	5.22	99.97	1	XRF
248-2A	73.32	0.10	13.14	0.95	0.04	0.01	0.47	3.10	5.34	96.48	13	EPM
248-8A	73.46	0.14	14.03	1.78	0.05	0.07	0.75	4.43	5.27	99.98	1	XRF
261-1A	74.13	0.13	11.61	1.96	0.06	0.11	0.68	2.42	3.90	95.03	2	EPM
<i>Obsidian Dome Tephra</i>												
OBS-1A	72.44	0.03	15.44	1.66	0.08	0.23	0.92	3.62	5.09	99.99	12	EPM
OBS-1B	69.00	0.31	17.41	1.53	0.09	0.38	1.41	4.83	5.00	99.96	7	EPM
OBS-2A	73.23	0.14	15.29	1.64	0.11	0.13	0.90	4.96	4.96	100.28	11	EPM
OBS-2B	70.33	0.17	14.15	1.65	0.04	0.13	0.81	3.26	4.12	94.66	4	EPM
OBS-3A	73.73	0.14	15.15	1.45	0.08	0.14	0.81	5.05	5.05	100.26	8	EPM
OBS-3B	69.28	0.34	16.97	1.97	0.07	0.34	1.62	4.55	4.19	99.33	7	EPM

*RhD, rhyodacite; Rhy, rhyolite; F-1, F-2, and F-3 refer to conduit fingers.

†FeO_x is reported as Fe₂O₃ for X ray fluorescence (XRF) analyses and as FeO for electron microprobe (EPM) analyses. Most of the individual pyroclasts are hydrated, accounting for the low totals for these analyses. EPM analyses are of small vesicular pyroclasts, whereas XRF analyses are of 1- to 4-cm-diameter obsidian clasts. Most of the fracture-filling pyroclasts are hydrated (Figure 5). XRF analyses are from the laboratory of P. Kyle, New Mexico Institute of Mining and Technology.

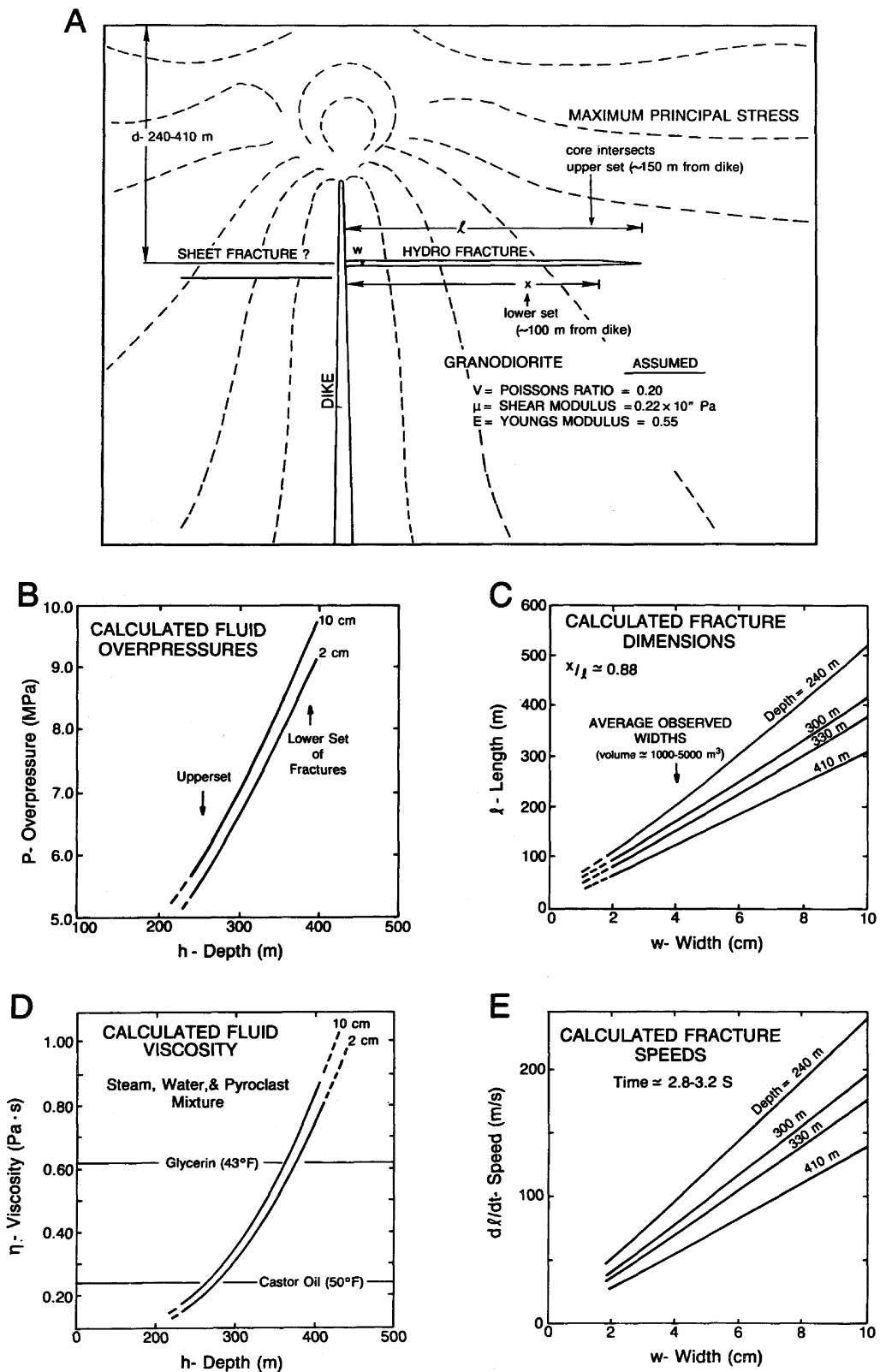


Fig. 10. A model of volcanic hydraulic fracturing. (a) Idealized sketch of the fracture geometry above and adjacent to a vertical dike. Note that hypothetical contours (dashed lines) of maximum principal stress are vertically oriented near the dike, which illustrates its possible influence upon the local stress field [Pollard *et al.*, 1983] and an explanation for the location of fractures encountered in the cores. (b) Calculated values of fluid overpressure needed to form the fractures. (c) Calculated fracture dimensions and average observed fracture widths. (d) Calculated fluid viscosities required to form the observed fractures. (e) Calculated fracture formation velocities.

range of possible viscosities (steam, water, and solid particulate slurry) and volume fluxes. Accordingly, we solve the appropriate equation set [Spence and Turcotte, 1985] for a cusplike crack tip to find temporal variations of fracture dimensions and viscosity variation with depth (Figures 10d and 10e), using earlier calculated spatial dimensions. Fracture propagation is shown to have taken several seconds, and fluid viscosity ranged from that of pure steam to that of a particle-laden saturated fluid.

The calculations assume that the fractured medium was previously nonfractured, that the fracturing occurred as a single event, and, as stated previously, that the fractures are horizontal. Fracture resistance is calculated to be small in relation to the viscous resistance of fluid flow in a crack of the observed dimensions (nondimensional stress intensity factor less than 1 [Spence and Turcotte, 1985]), even for cases of reduced shear modulus and critical stress intensity factor [Clifton et al., 1976]. Hence the calculated fracture fluid overpressures might be realistic despite the likelihood that the quartz monzonite was already fractured by exfoliation, faulting, or both. Still, the presence of sheet fractures may have played a critical role in localizing groundwater near the conduit and dike, which is necessary for creation of phreatomagmatic overpressures [Wohletz, 1986].

Multiple beds and erosion surfaces within fracture fillings provide evidence that the fracture extension occurred in pulses, consistent with the multitude of explosive events recorded in tephra sections at Obsidian Dome. The calculated fracture propagation speeds of 50 to 200 m/s indicate a total fracture propagation time of several seconds. If indeed numerous fracture pressurizations did occur, then individual fracture extension events took place in less than a second.

The Origin of Bedding Features in Fracture Fillings

Bedding within fracture fillings implies substantial fluid flow within those fractures. Chouet and Julian [1985] state that fluid flow is required for tensile failure to occur. Hydraulic fracturing experiments conducted in Nevada [Schmidt et al., 1981; Warpinski et al., 1981] involved the use of multiple injections, each time using a different color sand proppant. The mineback into these experimental fractures revealed the presence of the sand as distinct layers. Kern et al. [1959] discuss laboratory experiments in which sand proppants are injected into simulated fractures; cross bedding was observed to result from settling and erosion caused by "overflushing" during continued flow of fluids through the partly open crack.

Evidence for contact of fracture-filling material with hydrothermal fluids includes solution pits on glass clasts from fractures next to the conduit (Figure 5). Mineral and lithic clasts in the same deposits have a thin coating of an authigenic clay, most likely a smectite (Figure 5). Clasts within fracture fill deposits adjacent to the dike have fresh surfaces, presumably related to either their greater distance from the dike or that they are partly crystalline.

Origin of the Glass Pyroclasts

In his study of Obsidian Dome, Wohletz [1987] proposed that the eruption went through three stages: (1) it began with fragmentation and eruption of a highly vesicular melt, producing a Plinian pumice deposit; (2) this explosive activity may have disrupted an aquifer, initiating phreatomagmatic activity, which produced blocky glass pyroclasts with low vesicularity; and (3) extrusion of Obsidian Dome.

The pyroclasts found in fractures adjacent to the conduit and dike are similar in many respects to those in the phreatomagmatic tephra; they have blocky shapes and less than 30% vesicles. They also match in composition the rhyolitic component of the intrusive and erupted Obsidian Dome lavas and tuffs. They lack the rhyodacitic component that is abundant in all but the phreatomagmatic phases of the eruption [Heiken and Wohletz, 1985]. We, therefore, infer that these pyroclasts were injected into the fractures, and to some extent acted as natural proppants, during the phreatomagmatic phases of the Obsidian Dome eruption.

The abundant tabular feldspars of many intrusive pyroclasts are similar to quench crystals described by Lofgren [1974]. Following Lofgren's [1974] approach, the normative feldspar compositions listed in Table 4 might be interpreted to indicate supercooling of 30°–80°C in dike fractures and 0°–50°C in those near the conduit.

We know less about the fractures adjacent to the dike but suggest that they were injected during the phreatic eruptions that formed the craters located between Obsidian Dome and the Glass Creek Flow. If so, the fracturing was a relatively late event here also, as craters were late in relation to the tephra eruptions but preceded dome emplacement. The hyalocrystalline character of the pyroclasts also argues for a time delay of perhaps hours or days between establishment of an adjacent intrusion and development of the fractures, long enough to allow for significant heating and pressurization of the area around the intrusion.

Variations in glass pyroclast textures have several explanations. The proximity of sampled fillings to the conduit and dike places a constraint on the thermal regime. The amount of groundwater intruding the fractures also might have controlled quenching rate. Furthermore, quench textures may reflect conditions related to magma dewatering during cooling. Maintenance of high water pressures in the gas-tight environment around the dike (in contrast with the open conduit) may explain continuation of crystal growth after fragmentation.

The low vesicularity of pyroclasts in fracture fillings adjacent to the dike may have several explanations:

1. Interaction of magma with groundwater quenched the magma before complete vesicle growth was possible.
2. There was early, shallow vesiculation of relatively dry magma (~1 wt. % H₂O).
3. They were formed at a fairly advanced stage of degassing bubble collapse of the intrusion. The presence of considerable primary vesicularity at greater depths in the dike support this explanation.

Geothermal Implications of Natural Hydrofracturing

These results suggest that hydraulic fracturing of country rock may be a common phenomenon during many magmatic events. Obviously, fracturing increases the permeability of rocks, but not so obvious is its profound effect upon transfer of heat and chemical constituents of magma and country rock. Numerous authors develop the concept of ore deposition in fractured rocks by hydrothermal circulation, and a similar approach is considered important for formation of a geothermal reservoir. Eruption processes in general and phreatomagmatic activity in particular may play an important role in the development of such circulation systems. Consideration of the abundant data available for geothermal locations in the Latium volcanic region of Italy supports the foregoing proposition [Funicello et al., 1976]. Typically, geothermal reservoirs

in the Laticum region exist in limestone strata at depths up to several kilometers [Funicello and Parotto, 1978]. These same strata also host regional aquifers. Furthermore, where volcanic ejecta are found to have an abundance of fragments derived from these strata, the ejecta deposits are of phreatomagmatic origin. Drilling (e.g., at the Latera volcano) has demonstrated the increased fracture density under volcanoes with histories of phreatomagmatic eruptions. The end result of this natural hydrofracturing process is a magma heat source surrounded by fractured and saturated country rock, a geothermal reservoir.

Acknowledgments. Support for this work was received from the U.S. Department of Energy (DOE) Continental Scientific Drilling Program, through Institutional Supporting Research and Development of Los Alamos National Laboratory, and through DOE contract DE-AC04-76DP00789 at Sandia National Laboratories. We appreciate the constructive and helpful reviews by Scott Baldrige, Roy Bailey, Robert Tilling, and an anonymous reviewer; thank you for your time and patience.

REFERENCES

- Andersen, T., and H. Qvale, Pyroclastic mechanism for carbonatite intrusion: Evidence from the intrusives in the Fen central complex, southeastern Norway, *J. Geol.*, **94**, 762-769, 1986.
- Barenblatt, G. I., Mathematical theory of equilibrium cracks, *Adv. Appl. Mech.*, **7**, 55-129, 1962.
- Batchelor, G. K., *An Introduction to Fluid Dynamics*, Cambridge University Press, New York, 1967.
- Birch, F., Compressibility; elastic constants, *Handbook of Physical Constants*, edited by S. P. Clark, Jr., *Mem. Geol. Soc. Am.*, **97**, 97-173, 1966.
- Chouet, B., Dynamics of a fluid-driven crack in three dimensions by the finite difference method, *J. Geophys. Res.*, **91**, 13,967-13,992, 1986.
- Chouet, B., and B. R. Julian, Dynamics of an expanding fluid-filled crack, *J. Geophys. Res.*, **90**, 11,187-11,198, 1985.
- Clifton, R. J., E. R. Simonson, A. H. Jones, and S. J. Green, Determination of the critical-stress-intensity factor K_{Ic} from internally pressurized thick-walled vessels, *Exp. Mech.*, **16**, 233-238, 1976.
- Eichelberger, J. C., P. C. Lysne, C. D. Miller, and L. W. Younker, Research drilling at Inyo Domes, California: 1984 results, *Eos Trans. AGU*, **66**, 186-187, 1985.
- Eichelberger, J. C., C. R. Carrigan, H. R. Westrich, and R. H. Price, Nonexplosive silicic volcanism, *Nature*, **323**, 598-602, 1986.
- Fehler, M., Observations of volcanic tremor at Mount St. Helens volcano, *J. Geophys. Res.*, **88**, 3476-3484, 1983.
- Fink, J. H., Geometry of silicic dikes beneath the Inyo Domes, California, *J. Geophys. Res.*, **90**, 11,127-11,133, 1985.
- Foulger, G. L., and R. E. Long, Anomalous focal mechanisms: Tensile crack formation on an accreting plate boundary, *Nature*, **310**, 43-45, 1984.
- Funicello, R., and M. Parotto, Il substrato sedimentario nell'area dei Colli Albani (vulcano laziale), *Geol. Rom.*, **17**, 831-849, 1978.
- Funicello, R., E. Locardi, G. Lombardi, and M. Pratto, The sedimentary ejecta from phreatomagmatic activity and their use for location of potential geothermal areas, in *Proceedings of Geothermal Energy*, pp. 227-240, International Congress on Thermal Waters, Geothermal Energy and Vulcanism of the Mediterranean Area, Athens, 1976.
- Geertsma, J., and R. Haafkens, A comparison of the theories for predicting width and extent of vertical hydraulically induced fractures, *Trans. ASME*, **101**, 8-20, 1979.
- Green, A. E., On Boussinesq's problem and penny-shaped cracks, *Proc. Cambridge Philos. Soc.*, **45**, 251-257, 1949.
- Heiken, G., and K. Wohletz, *Volcanic Ash*, 246 pp., University of California Press, Berkeley, 1985.
- Howard, G. C., and C. R. Fast, *Hydraulic Fracturing*, Society of Petroleum Engineers of the American Institute of Mining, Metallurgical, and Petroleum Engineers, New York, 1970.
- Hubbert, M. K., and D. G. Willis, Mechanics of hydraulic fracturing, *Trans. Soc. Pet. Eng. AIME*, **210**, 153-166, 1957.
- Irwin, G. R., Analysis of stresses and strains near the end of a crack traversing a plate, *J. Appl. Mech.*, **24**, 361-364, 1957.
- Johnson, A. M., *Physical Processes in Geology*, Freeman, Cooper & Company, San Francisco, Calif., 1970.
- Julian, B. R., Evidence for dyke intrusion earthquake mechanisms near Long Valley caldera, California, *Nature*, **303**, 323-325, 1983.
- Julian, B. R., and S. A. Simpkin, Earthquake processes in the Long Valley caldera area, California, *J. Geophys. Res.*, **90**, 11,155-11,169, 1985.
- Kern, L. R., T. K. Perkins, and R. E. Wyant, The mechanics of sand movement in fracturing, *Trans. Soc. Pet. Eng. AIME*, **216**, 403-405, 1959.
- Kistler, R. W., Structure and metamorphism in the Mono Craters Quadrangle, Sierra Nevada, California, *U.S. Geol. Surv. Bull.*, **1221-E**, 55 pp., 1966.
- Lofgren, G., An experimental study of plagioclase crystal morphology: Isothermal crystallization, *Am. J. Sci.*, **274**, 243-273, 1974.
- Love, A. E. H., Boussinesq's problem for a rigid cone, *Q. J. Math.*, **10**, 161-175, 1939.
- Miller, C. D., Holocene eruptions at the Inyo volcanic chain, California: Implications for possible eruptions in Long Valley caldera, *Geology*, **13**, 14-17, 1985.
- Nairn, I. A., and S. Wiradiradja, Late Quaternary hydrothermal explosion breccias at Kawerau geothermal field, New Zealand, *Bull. Volcanol.*, **43**, 1-13, 1980.
- Nelson, C. E., and D. L. Giles, Hydrothermal eruption mechanisms and hot spring gold deposits, *Econ. Geol.*, **80**, 1633-1639, 1985.
- Norton, D. L., Theory of hydrothermal systems, *Annu. Rev. Earth Planet. Sci.*, **12**, 155-177, 1984.
- Pollard, D. D., P. T. Delaney, W. A. Duffield, E. T. Endo, and A. T. Okamura, Surface deformation in volcanic rift zones, *Tectonophysics*, **94**, 541-584, 1983.
- Schmidt, R. A., N. R. Warpinski, S. J. Finley, and R. C. Shear, Multi-frac test series: Final report, *Rep. SAND81-1234*, 183 pp., Sandia Natl. Lab., Albuquerque, N. Mex., 1981.
- Sheridan, M. F., K. W. Wohletz, and J. Dehn, Discrimination of grain-size subpopulations of pyroclastic deposits, *Geology*, **15**, 367-370, 1986.
- Spence, D. A., and D. L. Turcotte, Magma-driven propagation of cracks, *J. Geophys. Res.*, **90**, 575-580, 1985.
- Sun, R. J., Theoretical size of hydraulically induced horizontal fractures and corresponding surface uplift in an idealized medium, *J. Geophys. Res.*, **74**, 5995-6011, 1969.
- Warpinski, N. R., L. D. Tyler, W. C. Vollendorf, and D. A. Northrop, Direct observation of a sand-propped fracture, *Rep. SAND81-9225*, 63 pp., Sandia Natl. Lab., Albuquerque, N. Mex., 1981.
- Watson, B. N., Intrusive volcanic phenomena in southern and central Arizona, in *Southern Arizona Guidebook III*, edited by S. R. Tittley, pp. 147-154, Arizona Geological Society, Tucson, 1968.
- West, F. G., G. H. Heiken, E. F. Homuth, R. W. Peterson, B. M. Crowe, and K. H. Wohletz, Tilts associated with volcanic activity, Guadeloupe, French West Indies, *Rep. LA-7500-MS*, 10 pp., Los Alamos Natl. Lab., Los Alamos, N. Mex., 1978.
- Wohletz, K. H., Explosive magma-water interactions: Thermodynamics, explosion mechanisms, and field studies, *Bull. Volcanol.*, **48**, 245-264, 1986.
- Wohletz, K. H., Chemical and textural surface features of pyroclasts from hydromagmatic eruption sequences, in *Characterization and Quantification of Surface Features on Clastic and Pyroclastic Particles*, edited by J. R. Marshall, chap. 2-2, pp. 79-97, Hutchinson Press, San Francisco, Calif., 1987.

J. Eichelberger, Sandia National Laboratories, Division 1543, Albuquerque, NM 87185.

G. Heiken and K. Wohletz, Earth and Space Science Division, Los Alamos National Laboratory, MS D462, Los Alamos, NM 87545.

(Received May 18, 1987;
revised September 21, 1987;
accepted October 20, 1987.)